Front. Earth Sci. 2020, 14(3): 625–636
https://doi.org/10.1007/s11707-019-0796-2

RESEARCH ARTICLE

Improved Kalman filter method considering multiple factors and its application in landslide prediction

Qing LING[1,2], Wei QU (✉)[1], Qin ZHANG[1], Lingjie KONG[2], Jing ZHANG[1], Li ZHU[3]

1 College of Geology Engineering and Geomatics, Chang'an University, Xi'an 710064, China
2 School of Civil Engineering, Lanzhou University of Technology, Lanzhou 730050, China
3 Information Engineering University, Zhengzhou 450002, China

Abstract Landslides, seriously threatening human lives and environmental safety, have become some of the most catastrophic natural disasters in hilly and mountainous areas worldwide. Hence, it is necessary to forecast landslide deformation for landslide risk reduction. This paper presents a method of predicting landslide displacement, i.e., the improved multi-factor Kalman filter (KF) algorithm. The developed model has two advantages over the traditional KF approach. First, it considers multiple external environmental factors (e.g., rainfall), which are the main triggering factors that may induce slope failure. Second, the model includes random disturbances of triggers. The proposed model was constructed using a time series which consists of over 16-month of data on landslide movement and precipitation collected from the Miaodian loess landslide monitoring system and nearby meteorological stations in Shaanxi province, China. Model validation was performed by predicting movements for periods of up to 7 months in the future. The performance of the developed model was compared with that of the improved single-factor KF, multi-factor KF, multi-factor radial basis function, and multi-factor support vector regression approaches. The results show that the improved multi-factor KF method outperforms the other models and that the predictive capability can be improved by considering random disturbances of triggers.

Keywords landslide, improved Kalman filter, triggering factors, displacement prediction

1 Introduction

Landslides have become some of the main natural hazards in hilly and mountain areas and caused casualties and economic damage worldwide. In addition to direct and indirect financial losses, landslides have also caused significant environmental damage (Huang, 2007; Cojean and Caï, 2011; Bai et al., 2012). Therefore, predicting landslide movements for early warnings is crucial to avoiding or at least mitigating adverse effects not only on humans and property but on the environment, especially when countermeasures are ineffective (Krkač et al., 2017). However, the landslide evolution process is nonlinear and complicated (Huang, 2004). Further landslides are generally considered to be governed by numerous internal and external factors known and unknown, e.g., geological conditions, rainfall intensity, and groundwater level fluctuations, showing stochastic behavior due to the stochastic characteristics of the triggers. Consequently, the randomness of landslides and external triggering factors as well as their complex nonlinear interrelationships make precise landslide displacement prediction a challenging task.

The stability of land is generally evaluated by displacement and displacement velocity during slope failure. Numerous landslide prediction models based on displacement have been developed since the proposal of empirical formulas presented by Saito (Saito, 1965; Fukuzono, 1985; Crosta and Agliardi, 2003; Polykretis et al., 2015; An et al., 2016; Carlà et al., 2017; Zhou et al., 2018). These approaches can be broadly grouped into three categories. The first category includes approaches based on creep theory, such as tertiary creep (Saito, 1965), and a model derived from the linear trend of an inverse displacement-rate curve (Voight, 1988 and 1989). The second category contains statistical techniques based on the displacement versus time, e.g., the gray model (Gao and Feng, 2006; Xu

Received December 4, 2018; accepted October 7, 2019

E-mail: maikerqq@163.com

et al., 2011), exponential smoothing model (De Livera et al., 2011), and Verhulst model (Yan, 1988; Li et al., 2012). The third category consists of nonlinear and artificial intelligence models, such as artificial neural networks (Pradhan and Lee, 2010; Alimohammadlou et al., 2014; Xu and Niu, 2018), the support vector machine model (Xu et al., 2012; Pradhan, 2013; Chen et al., 2016; Hong et al., 2016), the radial basis function (RBF) model (Li et al., 2008), and various coupling models (Wu et al., 2007; Liu et al., 2014; Tazik et al., 2014; Zhang et al., 2015; Bui et al., 2016; Colkesen et al., 2016; Huang et al., 2016; Miao et al., 2018).

Among the mentioned techniques above, the Kalman filter (KF) approach has been widely applied to solving dynamic deformation data in landslide predictions because it has the best linear unbiased estimator, is easy to program, and has a low memory requirement (Li et al., 2010; Qian et al., 2012; Zhang et al., 2012; Fu, 2013; Lu and Jiang, 2017). However, the factors triggering landside deformation are not considered in the traditional KF model, which results in a poor performance. Hence, landslide predictions with improved accuracy are never achieved by considering only the displacement since landslides are influenced by various factors such as rainfall and underground water level variation (He et al., 2010; Zou et al., 2017). To overcome this limitation, an improved multi-factor KF technique based on the random disturbances of external triggers is presented to yield strong function fitting and generalization ability for improved accuracy. In addition, landslide displacement is generally divided into three terms — trend terms, periodical components, and random terms and each of which can be predicted separately (Cao et al., 2016; Zhou et al., 2018). However, although simulation is much more complex, most models only predict the trend terms and periodical components, ignoring the influence of random terms (Xu and Niu, 2018; Zhou et al., 2018). Therefore, without decomposing the displacement, this report presents an improved multi-factor KF model considering the random disturbances of external factors. These factors have not been studied previously, and no such model has been proposed previously. The Jingyang landslide in Shaanxi province of China was taken as a case study. Based on the analysis of landslide deformation, the monthly rainfall and daily maximum precipitation were selected as the triggering factors of landslide movements. To verify the performance of the proposed model (the improved multi-factor KF approach), the improved single-factor KF, multi-factor KF, multi-factor RBF, and multi-factor SVR models were applied to predict landslide displacement for comparison. The results show that the developed model performs better than the other models considered in this study.

2 Method

2.1 KF algorithm

Consider a linear dynamic system (Cui et al., 2009)

$$\begin{cases} \hat{X}_k = \Phi_{k,k-1}\hat{X}_{k-1} + \Gamma_{k,k-1}\Omega_{k-1} \\ L_k = B_k\hat{X}_k + \Delta_k \end{cases}, \quad (1)$$

where $\hat{X}_k$ is the state vector at epoch k and $\hat{X}_{k-1}$ is the state vector at epoch $k-1$, $\Phi_{k,k-1}$ is the state transition matrix, $\Gamma_{k,k-1}$ is the coefficient matrix of the state noise Ω_{k-1}, L_k is the observation at epoch k, and B_k is the observation matrix. The symbols Ω_{k-1} and Δ_k are the state noise and measurement noise respectively, both of which are zero mean uncorrelated Gaussian white noise satisfying

$$E[\Omega_k\Omega_j^{\mathrm{T}}] = Q_k\delta_{kj}, E[\Delta_k\Delta_j^{\mathrm{T}}] = R_k\delta_{kj}, E[\Omega_k\Delta_j^{\mathrm{T}}] = 0, \quad (2)$$

where Q_k and R_k are the corresponding covariances of Ω_{k-1} and Δ_k respectively, and δ_{kj} is the Kronecker delta function.

Then, the main KF equations are as follows (Yang et al., 2001, 2006, 2010):
Prediction:

$$\begin{aligned} \hat{X}_{k/(k-1)} &= \Phi_{k,k-1}\hat{X}_{k-1}, \\ D_{\hat{X}_{k/(k-1)}} &= \Phi_{k,k-1}D_{\hat{X}_{k-1}}\Phi_{k,k-1}^{\mathrm{T}} + \Gamma_{k,k-1}D_{\Omega_{k-1}}\Gamma_{k,k-1}^{\mathrm{T}}, \end{aligned} \quad (3)$$

Updating:

$$\begin{aligned} J_k &= D_{\hat{X}_{k/(k-1)}}B_k^{\mathrm{T}}(B_kD_{\hat{X}_{k/(k-1)}}B_k^{\mathrm{T}} + D_{\Delta_k})^{-1} \\ \hat{X}_k &= \hat{X}_{k/(k-1)} + J_k(L_k - B_k\hat{X}_{k/(k-1)}) \\ D_{\hat{X}_k} &= (I - J_kB_k)D_{\hat{X}_{k/(k-1)}} \end{aligned} \quad (4)$$

where $\hat{X}_{k/(k-1)}$ is the predicted state vector; $D_{\hat{X}_{k/(k-1)}}$ is the variance matrix of $\hat{X}_{k/(k-1)}$; J_k is the gain matrix; $D_{\Omega_{k-1}}$ represents the variance matrix of the state noise Ω_{k-1}; D_{Δ_k} stands for the variance matrix of the measurement noise Δ_k; $\hat{X}_k$ is the estimated state; $D_{\hat{X}_k}$ is the variance matrix of $\hat{X}_k$; and $D_{\hat{X}_{k-1}}$ is the variance matrix of $\hat{X}_{k-1}$.

2.2 Modified KF considering multiple factors

According to the geological conditions in the study area, the monthly rainfall and daily maximum precipitation were chosen as the main triggering factors (Duang, 2013; He, 2016). Hence, the deformation model can be further expressed as

$$x = x(t,\ r,T), \tag{5}$$

where t is the observation time, r is the monthly cumulative rainfall, T is the daily maximum precipitation in a month, and x is the monthly landslide deformation.

The short interval of observation time and small deformation means that the Taylor series expansion of x can be obtained as follows (excluding the cubic terms):

$$\begin{aligned} x_k(t_k,r_k,T_k) = {} & x_{k-1}(t_{k-1},r_{k-1},T_{k-1}) + v_{k-1}(t_k - t_{k-1}) \\ & + a_{k-1}(t_k - t_{k-1})^2 + b_{k-1}(r_k - r_{k-1}) \\ & + c_{k-1}(r_k - r_{k-1})^2 + d_{k-1}(T_k - T_{k-1}) \\ & + e_{k-1}(T_k - T_{k-1})^2, \end{aligned} \tag{6}$$

where $v_{k-1} = \left(\frac{\partial x}{\partial t}\right)_{t_{k-1}}$ is the deformation velocity of the landslide at epoch t_{k-1}, $a_{k-1} = \frac{1}{2}\left(\frac{\partial x}{\partial t}\right)^2_{t_{k-1}}$ is the deformation acceleration of the landslide at epoch t_{k-1}, $b_{k-1} = \left(\frac{\partial x}{\partial r}\right)_{r_{k-1}}$ is the influence of rainfall on the landslide, $c_{k-1} = \frac{1}{2}\left(\frac{\partial x}{\partial r}\right)^2_{r_{k-1}}$ is the random disturbance of rainfall, $d_{k-1} = \left(\frac{\partial x}{\partial T}\right)_{T_{k-1}}$ is the impact of daily maximum precipitation on the landslide, and $e_{k-1} = \frac{1}{2}\left(\frac{\partial x}{\partial T}\right)^2_{T_{k-1}}$ is the random disturbance of daily maximum precipitation.

Given the random disturbance of external factors and regarding the acceleration as dynamic noise (Cui et al., 2009; Lu and Jiang, 2017), the coefficient matrix of the state noise can be written as

$$\Gamma_{k,k-1} = \int_{t_{k-1}}^{t_k} \Phi(t_k,\tau)F(\tau)\mathrm{d}\tau = \left[\frac{1}{6}\Delta t_{k-1}^3 + \frac{1}{2}\Delta r_{k-1}^2\Delta t_{k-1} + \frac{1}{2}\Delta T_{k-1}^2\Delta t_{k-1}\ \ \Delta r_{k-1}\Delta t_{k-1}\quad \Delta t_{k-1}\quad \Delta T_{k-1}\Delta t_{k-1}\quad \Delta t_{k-1}\right]^{\mathrm{T}},$$

where

$$F(\tau) = [0\quad 0\quad 1\quad 0\quad 1\quad 0\quad 1]^{\mathrm{T}}.$$

The state equation can be expressed as follows:

$$\begin{bmatrix} x_k \\ v_k \\ a_k \\ b_k \\ c_k \\ d_k \\ e_k \end{bmatrix} = \begin{bmatrix} 1 & \Delta t_{k-1} & \frac{1}{2}\Delta t_{k-1}^2 & \Delta r_{k-1} & \frac{1}{2}\Delta r_{k-1}^2 & \Delta T_{k-1} & \frac{1}{2}\Delta T_{k-1}^2 \\ 0 & 1 & \Delta t_{k-1} & 0 & 0 & 0 & 0 \\ 0 & 0 & 1 & 0 & 0 & 0 & 0 \\ 0 & 0 & 0 & 1 & \Delta r_{k-1} & 0 & 0 \\ 0 & 0 & 0 & 0 & 1 & 0 & 0 \\ 0 & 0 & 0 & 0 & 0 & 1 & \Delta T_{k-1} \\ 0 & 0 & 0 & 0 & 0 & 0 & 1 \end{bmatrix} \begin{bmatrix} x_{k-1} \\ v_{k-1} \\ a_{k-1} \\ b_{k-1} \\ c_{k-1} \\ d_{k-1} \\ e_{k-1} \end{bmatrix} + \begin{bmatrix} \frac{1}{6}\Delta t_{k-1}^3 + \frac{1}{2}\Delta r_{k-1}^2\Delta t_{k-1} + \frac{1}{2}\Delta T_{k-1}^2\Delta t_{k-1} \\ \frac{1}{2}\Delta t_{k-1}^2 \\ \Delta t_{k-1} \\ \Delta r_{k-1}\Delta t_{k-1} \\ \Delta t_{k-1} \\ \Delta T_{k-1}\Delta t_{k-1} \\ \Delta t_{k-1} \end{bmatrix} \Omega_{k-1}, \tag{7}$$

where $\hat{X}_k = [x_k\quad v_k\quad a_k\quad b_k\quad c_k\quad d_k\quad e_k]^{\mathrm{T}}$, $\Delta t_{k-1} = t_k - t_{k-1}$, $\Delta r_{k-1} = r_k - r_{k-1}$, $\Delta T_{k-1} = T_k - T_{k-1}$, and

$$\Phi_{k,k-1}=\begin{bmatrix}1 & \Delta t_{k-1} & \frac{1}{2}\Delta t_{k-1}^2 & \Delta r_{k-1} & \frac{1}{2}\Delta r_{k-1}^2 & \Delta T_{k-1} & \frac{1}{2}\Delta T_{k-1}^2\\ 0 & 1 & \Delta t_{k-1} & 0 & 0 & 0 & 0\\ 0 & 0 & 1 & 0 & 0 & 0 & 0\\ 0 & 0 & 0 & 1 & \Delta r_{k-1} & 0 & 0\\ 0 & 0 & 0 & 0 & 1 & 0 & 0\\ 0 & 0 & 0 & 0 & 0 & 1 & \Delta T_{k-1}\\ 0 & 0 & 0 & 0 & 0 & 0 & 1\end{bmatrix}.$$

Equation (7) can be written as

$$\hat{X}_k=\Phi_{k,k-1}\hat{X}_{k-1}+\Gamma_{k,k-1}\Omega_{k-1}. \tag{8}$$

The observed equation is

$$L_k=BX_k+\Delta_k, \tag{9}$$

where L_k represents the deformation at the epoch k, $B_k=[1\quad 0\quad 0\quad 0\quad 0\quad 0\quad 0]$.

2.3 Proposed model and performance evaluation

In this study, the total displacement and precipitation data were modeled into the improved multi-factor KF. The performance of the proposed method was compared with those of the improved single-factor KF, multi-factor KF, multi-factor RBF, and multi-factor SVR approaches.

Four statistical indices were adopted to assess the model performance: the root mean square error (RMSE), absolute percentage error (APE), mean absolute percentage error (MAPE), and goodness of fit (R^2). Larger values of R^2 and smaller values of the *RMSE* and *MAPE* indicate higher prediction performance. The formulas used to calculate these four measures are as follows:

$$RMSE=\sqrt{\frac{1}{n}\sum_{i=1}^{n}\left(\hat{L}_i-L_i\right)^2}, \tag{10}$$

$$APE=\left|\frac{\hat{L}_i-L_i}{L_i}\right|, \tag{11}$$

$$MAPE=\frac{1}{n}\sum_{i=1}^{n}\left|\frac{\hat{L}_i-L_i}{L_i}\right|, \tag{12}$$

$$R^2=\frac{\left(n\sum_{i=1}^{n}\hat{L}_iL_i-\sum_{i=1}^{n}\hat{L}_i\sum_{i=1}^{n}L_i\right)^2}{\left(n\sum_{i=1}^{n}\hat{L}_i{}^2-\left(\sum_{i=1}^{n}\hat{L}_i\right)^2\right)\left(n\sum_{i=1}^{n}L_i{}^2-\left(\sum_{i=1}^{n}L_i\right)^2\right)}, \tag{13}$$

where n is the cumulative number of displacements, L_i is the observed displacement, and $\hat{L}_i$ is the predicted displacement.

3 Case study with real landslide monitoring data

3.1 Regional geological structure

We selected a landslide in the world-famous Loess Plateau as research object to test the effectiveness of the new KF algorithm. The study area is in the Jingyang region, Shaanxi province of central China (Fig. 1). Numerous landslides have developed in the Jingyang region with a generally stripped distribution along the right bank of the Jing River. By the end of April 2016, 92 loess landslides had occurred at 69 locations in the study area, 17 of which slid two or more times (Duang, 2013; He, 2016). In the region from Jiangliu to Miaodian, 64 slope failures occurred (He, 2016). Furthermore, there have been 34 landslides in the area from Zhaitou to Miaodian, within a distance of only 3.6 km (He, 2016).

In the study area, the front part of the landslide is 700 m away from Jing River, whereas the back part is 60 m away from a diversion canal with elevation ranging from 470 m to 370 m (Liu et al., 2017). The study area has an average longitudinal dimension of ~267 m, a width of ~227 m with the main sliding direction oriented at ~14°, and a forward sliding distance of ~300 m. Due to the continuous lateral erosion of the Jing River, a high and steep slope with a height of ~50 m and a gradient of ~60° has gradually developed, and a relatively open alluvial-diluvial terrace has formed. Irregular concave terrain exists on both sides of the landslide. In addition, the formation of three free surfaces of the soil has been accomplished owing to frequent occurrences of landslides in the study area, providing natural topographic conditions for the development of loess landslides (Fig. 2).

Geologically, the study area consists of Malan loess, Lishi loess, and Paleosol (Fig. 2). The loess layer is relatively loose and has well-developed vertical joints with strong permeability, while Paleosol is relatively waterproof or weakly permeable. The vertical infiltration of precipitation from the upper part of the slope into the soil results in an increase in saturation and a decrease in the shear

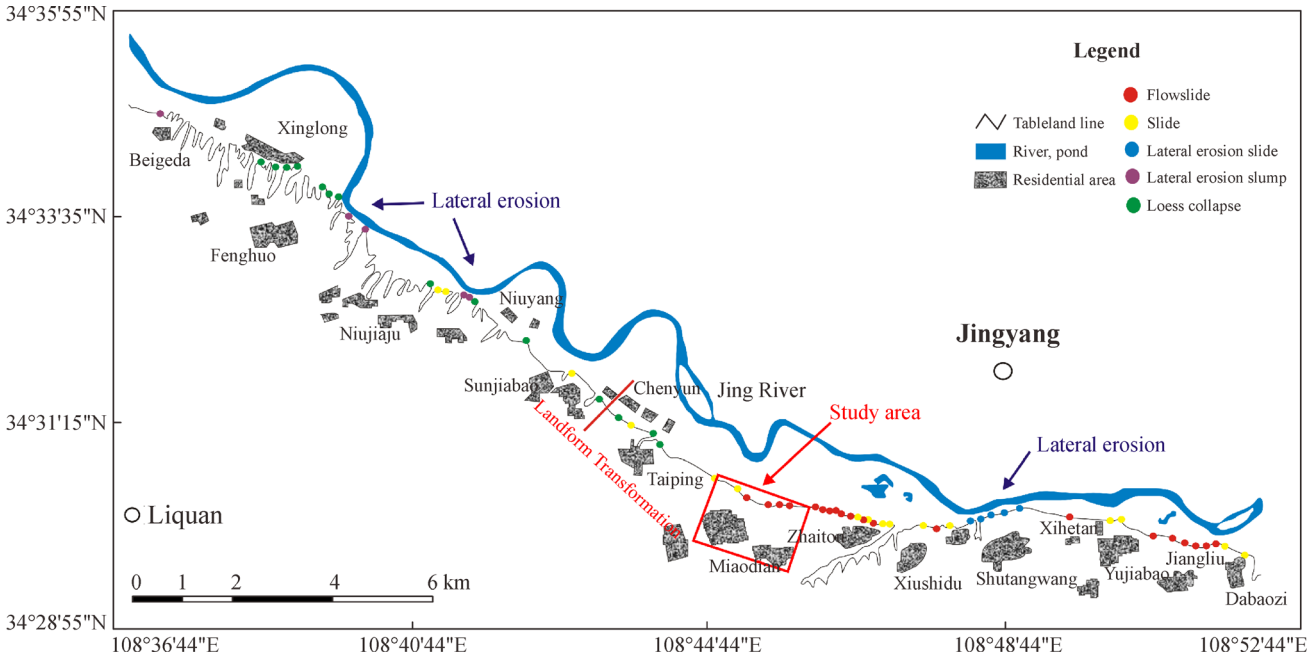

Fig. 1 Geographic locations of the Jingyang landslides.

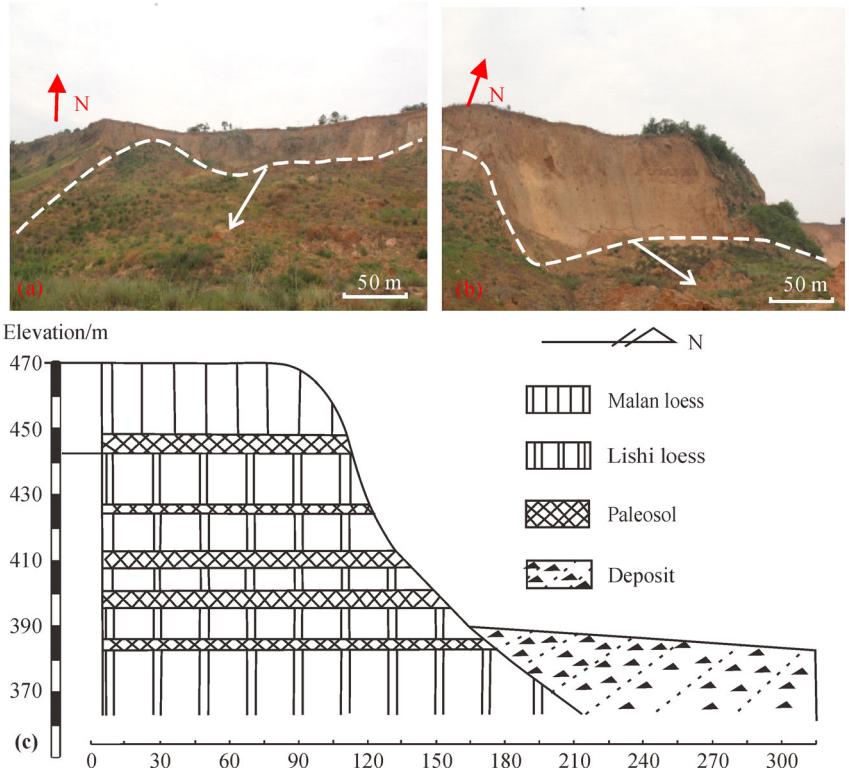

Fig. 2 Landslide in the study area (Photos were taken on December 5, 2015). (a) Landslides that occurred in 2013; (b) Landslide that occurred on May 26, 2015; (c) geological profile of Miaodian landslide.

strength of the contact surface, thus promoting the development of a weak sliding surface. Further, the tendency of the soil layer is consistent with that of the slope, which accelerates the deformation and consequently

failure of the slope. Geographically, the study area is in a temperate continental monsoon region that receives 548.7 mm of rainfall annually and has temperatures ranging from below 20.8°C to 41.8°C. Since the 1970s, more than 80 landslides have occurred at 30 locations in the south Plateau of Jingyang, 3 of which are within the study area (Liu et al., 2017). Closely related to external factors (e.g., rainfall), the groundwater level in the landslide zones widely varies with seasonal rainfall and irrigation, which are also among the main triggering factors affecting landslide stability (Cao et al., 2016).

Thus, the steep slopes and fronts of landslides provide favorable terrain conditions for slope deformation. After heavy precipitation a large quantity of rainwater infiltrates the soil layer, increasing the bulk density of the soil and decreasing its shear strength, thus adversely impacting the overall stability of the land.

3.2 Temporal evolution characteristics of landslide deformation

To effectively evaluate the slope stability of the study area, a deformation monitoring network was constructed in June 2015 (Fig. 3). Nine monitoring stations denoted MD01–MD09 were established in the landslide area. Three stations (JZ01, JZ02, and JZ03) established on stable regions were used as the data. Deformation monitoring with high precision (plane precision better than ±5 mm, height precision better than ±3 mm) was frequently conducted by employing the Leica TS30 measurement robot (Switzerland). At present, landslide deformation data from June 2015 to May 2017 are available.

Figure 4 presents the monitoring data obtained at nine stations from July 2015 to May 2017. The results demonstrate that each point deformed to a different degree, where MD09 experienced significant S-shaped deformation. The cumulative settlement of MD09 was up to −582 mm until May 2017. In the initial stage, the displacement of MD09 increased slowly. The displacement then became faster before gradually slowing down. This deformation characteristic of MD09 is very representative. In addition, MD09 was located at the edge of the middle of the landslide, and this area is prone to deformation under favorable conditions. Hence, MD09 was selected for detailed analysis due to its typical deformation and location.

Previous researchers have revealed that slope failure is never attributable to only one single cause, but rather a collection of parameters that contribute in an interactive manner (Yalcin et al., 2011). According to this argument, landslides occur due to the comprehensive and mutual influences of various factors that account for the frequent occurrences of landslides. In this section, the triggering factors will be discussed to explore the failure mechanisms. Data on monthly displacement, daily maximum rainfall, and monthly cumulative precipitation at MD09 are shown in Fig. 5, and the relationships among these factors were analyzed and presented as follows.

The stage between July and October 2015 was immediately after the slope failure occurred in June

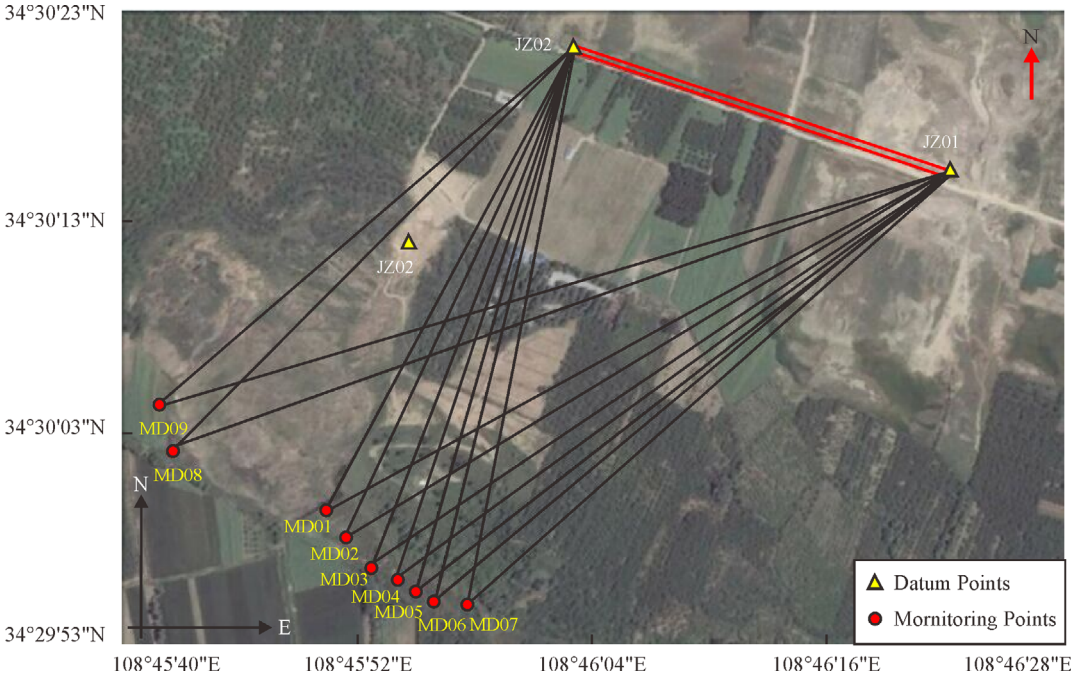

Fig. 3 Deformation monitoring network of landslides in the study area.

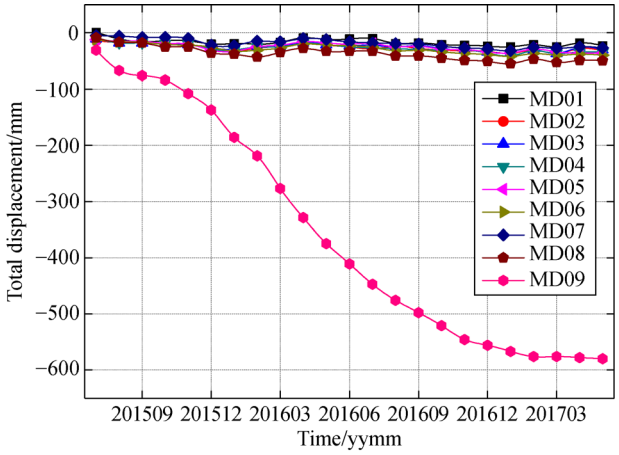

Fig. 4 Monitoring curves for accumulated displacement of landslides at 9 monitoring stations.

2015. Energy dissipation occurred, and the rate of deformation gradually became stable after reaching its peak value in August. Therefore, although the rainfall was intense, the landslide was in a stable state and underwent little deformation.

From November 2015 to May 2016, precipitation was gentle but deformation was relatively high, and this is probably due to the irrigation in winter (early November–late December) and spring (early March–mid-April) (Fig. 5). Widespread irrigation may have caused prompt rebounding of the groundwater, inducing uplift pressure. Furthermore, the high saturation at the beginning of irrigation would have led to obvious vertical subsidence of the landslide, rapidly increasing the vertical displacement. In addition, as the groundwater generated by seasonal freeze-thaw discharge was blocked, the groundwater level tended to increase; this induced a large vertical subsidence. When factors such as precipitation and irrigation are superimposed, the stability of the landslide will be affected and the cumulative displacement will increase significantly (Jing and Dai, 2007; Li et al., 2007; Wang and Yao, 2008). For instance, periods such as November–December 2015, March–April 2016, July–August 2016, and November–December 2016 show similar patterns (Fig. 5). In addition, precipitation slows landslide deformation. It is clear that large movements in November 2015 were also attributable to the rainfall in the previous month, when precipitation reached 60.2 mm. The displacement in November 2016 also showed similar patterns. Thus, the deformation is mainly attributable to the interaction of widespread irrigation and the effects of precipitation during this stage.

From June 2016 to February 2017, the monthly displacement exhibits good agreement with the variations in the monthly rainfall intensity and daily maximum rainfall intensity in a month (Fig. 5). From Fig. 5, it is obvious that the cumulative displacement increases in a hopping and fluctuating manner along with the precipitation to a certain extent. However, in September and December 2016, the rainfall was gentle, whereas the landslide experienced substantial movement. As discussed above, the hysteresis impact of precipitation on the displacement accounts for the large deformation since there was strong rainfall in the previous two months, i.e., August and November. Furthermore, widespread winter irrigation from early November to late December corresponds to the large deformation in December 2016. The correlation coefficient between the displacement and monthly rainfall was found to be 0.79 and 0.88 during this period with and without considering the data from September and December 2016, respectively. Hence,

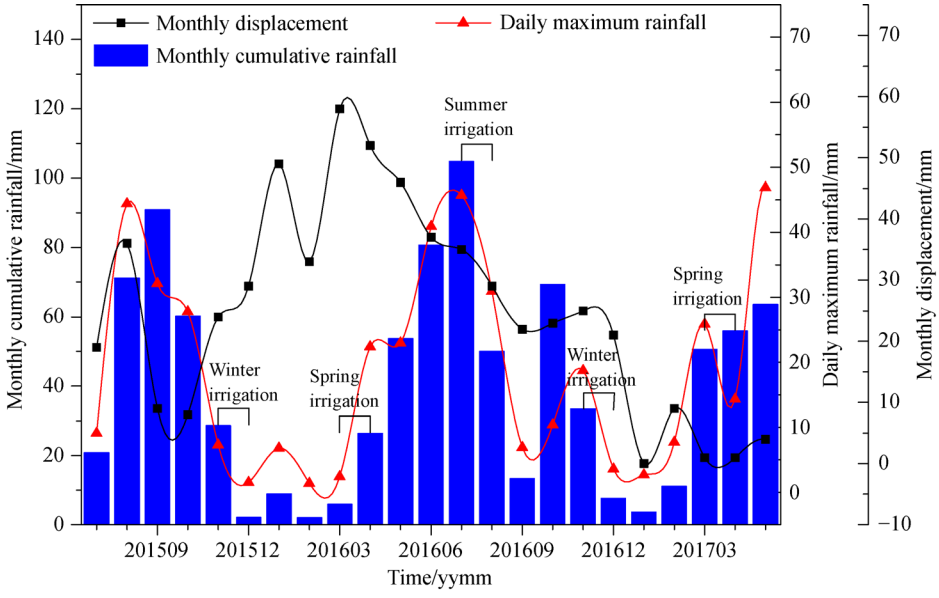

Fig. 5 Monthly cumulative rainfall, daily maximum precipitation and monthly displacement monitoring data of station MD09.

precipitation was the main external factor that influenced landslide movement during this time and exerted a "lagged effect" on landslide deformation to some extent, and widespread irrigation also contributed substantially to slope failure.

Since canal renovation was completed from March to May 2017, widespread irrigation had minimal influence on landslide stability. Additionally, even though the precipitation was heavy, the landslide experienced little deformation, demonstrating that the landslide was in a stable state. Thus, the increase in landslide displacement generally became stable despite the dramatic increase in precipitation.

In the light of the abovementioned qualitative and quantitative analysis, obvious nonlinear dynamic response relationships were observed between external triggers and landslide displacement in the study area. A combination of parameters, e.g., rainfall variations and widespread irrigation, contributed interactively to the occurrence of landslides, and seasonal freeze-thaw also had adverse influences on landslide stability.

3.3 Modeling and prediction of landslide displacement

Based on the analysis of the Jingyang landslide, the predictive multi-factor KF was proposed to establish a predictive model of landslide movement in the study area. Monitoring data for the period from July 2015 to October 2016 were selected to establish the model, and those from November 2016 to May 2017 were employed for validation. The monthly cumulative rainfall and daily maximum rainfall were selected as the main triggering factors to simulate and predict landslide deformation accurately. Further, to analyze the efficiency of the improved multi-factor KF, four other methods were adopted to predict the displacement: the improved single-factor KF, multi-factor KF, multi-factor RBF, and multi-factor SVR approaches. The R^2, *RMSE*, and *MAE* of all the models discussed are shown in Table 1.

Table 1 The displacement forecasting performance of improved multi-factors KF, improved single-factor KF, multi-factors KF, multi-factors RBF and multi-factors SVR

Models	R^2	*RMSE*/mm	*MAPE*/%
Improved multi-factor KF	0.976	4.608	0.7
Improved single-factor KF	0.941	8.405	1.1
Multi-factor KF	0.974	11.218	2.0
Multi-factor RBF	0.899	12.14	2.0
Multi-factor SVR	0.914	36.34	5.24

From Table 1 and Fig. 6, it is clear that the predictions of all considered models agree closely with the measurements, where the improved multi-factor KF approach performs better than the other mentioned techniques. The highest R^2 value of 0.976 was also achieved using the proposed model. Considering the predictions, the lowest *RMSE* and *MAPE* values were obtained with the proposed method. Specifically, the *RMSE* and *MAPE* were found to be 4.608 mm and 0.7%, respectively, with the improved multi-factor KF model; 8.405 mm and 1.1%, respectively, with the improved single-factor KF technique; 11.218 mm and 2.0%, respectively, with the multi-factor KF approach; 12.14 mm and 2.0%, respectively, with the multi-factor RBF method; and 36.34 mm and 5.24%, respectively, with the multi-factor SVR method. Thus, the developed technique was determined to be the optimal model in this study.

Additionally, although the three compared models performed well most of the time, all of them achieve less accurate prediction as the number of prediction test samples increases while the proposed approach still shows higher accuracy in the prediction of landslide movements. For instance, the APE of the proposed model from March to May 2017 is only 0.01%, 0.62%, and 0.73% (Fig. 7), whereas the APE of the improved single-factor KF, multi-factor KF, multi-factor RBF and multi-factor SVR are 2.23%, 2.31%, and 1.99%; 2.13%, 1.41%, and 1.77%; 0.28%, 2.11%, and 2.52%; and 7.22%, 9.38%, and 10.29%, respectively (Fig. 7).

Furthermore, the multi-factor KF model can also predict the general trend of landslide deformation with $R^2 = 0.974$ and *RMSE* = 11.218 mm. However, when it comes to the critical period (from December 2016 to February 2017), the predicted displacements vary greatly from the measurements. The maximum APE of the multi-factor KF is found to be 2.49% in February, while that of the proposed model is only 1.14%, which reveals that the developed technique performs better than the multi-factor KF approach. The random disturbance of external factors modeled in the proposed technique explains the more desirable predictions. The comparison revealed that the prediction performance of the multi-factor KF approach cannot surpass that of the improved multi-factor KF model, which yielded higher APE values than our proposed model. The developed method achieves high accuracy both in model fitting and prediction (Fig. 8). Hence, this study reveals that the improved multi-factor KF technique, which reflects the relationship between the triggers and displacement more accurately and considers the disturbances of the external triggering factors, is the most promising approach among the considered models. In addition, highly precise predictions for the next seven months could be achieved by using the improved multi-factor KF model without decomposing the initial data, enabling researchers to forecast landslide movements more accurately.

3.4 Discussion

In this study, to obtain accurate landslide movement predictions for landslide risk reduction, a predictive model, i.e., the improved multi-factor KF approach, was devel-

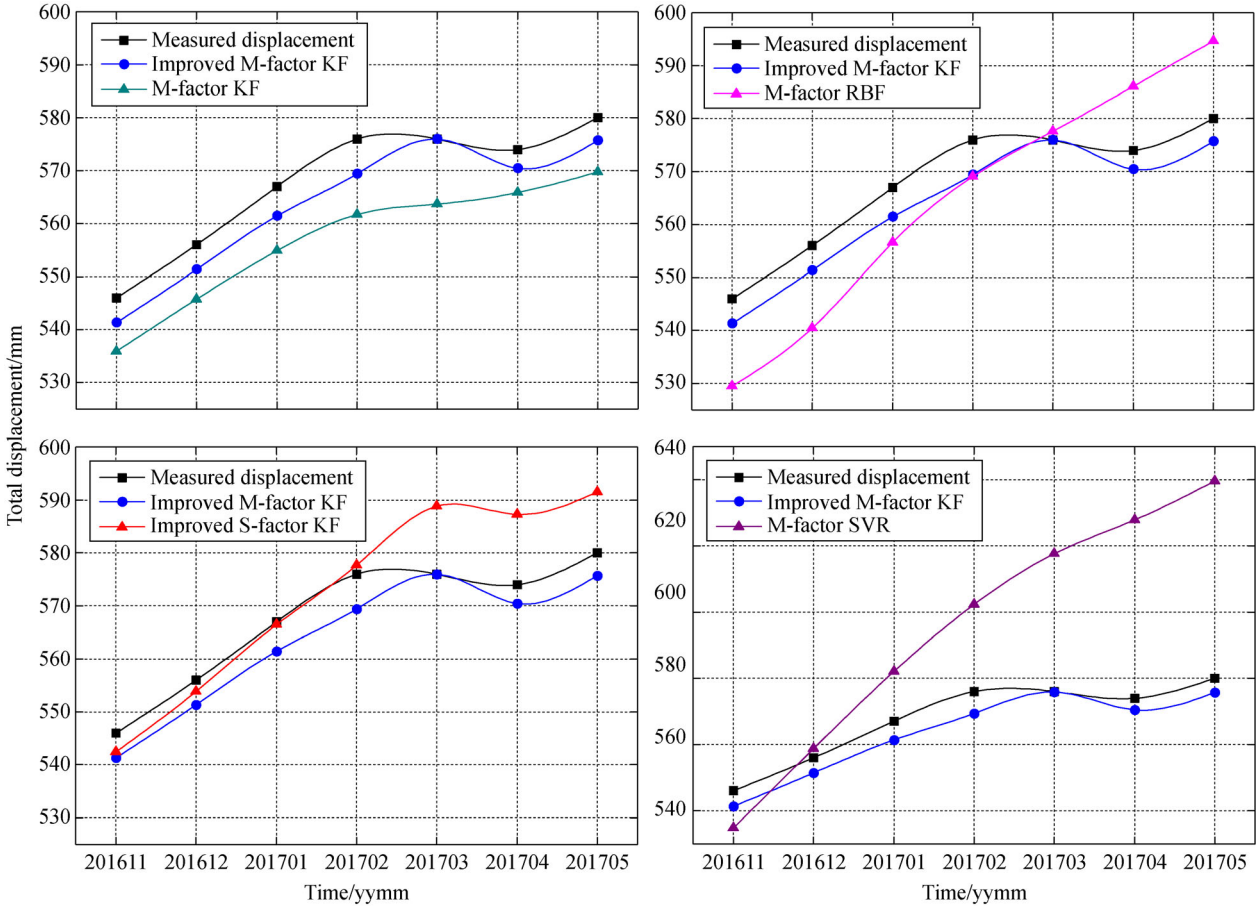

Fig. 6 The total displacement prediction adopting the improved multi-factors KF, the improved single-factor KF, multi-factors KF, multi-factors RBF and multi-factors SVR models (M-factors means multi-factors, and S-factor means single-factor).

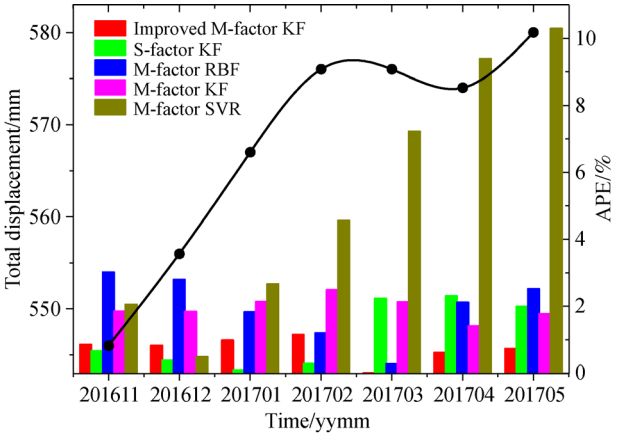

Fig. 7 The APE of the improved multi-factors KF (Improved M-factor KF), the improved single-factor KF (S-factor KF), multi-factors KF (M-factor KF), multi-factors RBF (M-factor RBF) and multi-factors SVR (M-factor SVR) models.

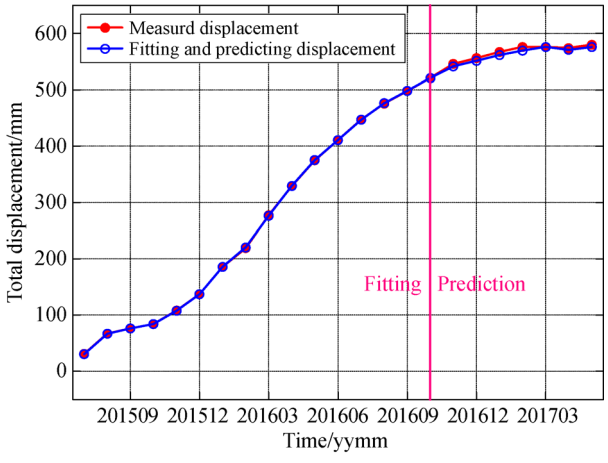

Fig. 8 Fitting and predicting displacement of MD09 using the improved multi-factors KF.

oped by considering the random disturbances of external triggering factors. The original data, consisting of more than 2 years of Miaodian landslide monitoring data, were subdivided into a training data set, which was used to calculate the equation parameters, and a validation data set,

which was employed to compare the prediction performances of the multi-factor KF approach, improved single-factor KF technique, and traditional approaches such as the SVR and RBF methods. The proposed model was verified based on statistical indices such as R^2, *RMSE*, *MAPE*, and *APE*.

The comparison of the aforementioned models revealed that the multi-factor KF can also achieve accurate predictions without considering the random disturbances of external factors, but inaccurate predictions occur especially in critical periods, resulting in the risk of misdirecting the decisions of disaster managers. Consequently, to obtain more accurate predictions, we propose the improved multi-factor KF with incorporation of random disturbance of external factors. The numerical results show that the proposed technique has prediction capabilities superior to those of the multi-factor KF model.

In addition, as shown in Figs. 6 and 7, the improved single-factor KF performed worse from March to May 2017, indicating that the improved single-factor KF cannot simulate the relationship between the deformation and triggers. Hence, the triggering factors should be considered for improved performance and accuracy.

Further, it can be seen from Fig. 6 that although the predictions reflect the general behaviors of the measurements, most of the predictions are smaller than the measurements. According to the collected geological data, this trend may be attributable to the influences of irrigation in winter and seasonal freeze-thaw, which were not modeled in the proposed technique due to the lack of underground water data resulting from limited monitoring conditions. However, even though the performance of the proposed model is not completely satisfactory since the effects of these factors (irrigation and seasonal freeze-thaw) are not included in the model, the overall predictions of the improved multi-factor KF model are still highly desirable. The effects of irrigation on slope stability should be incorporated into the proposed technique for improved accuracy in the future.

Therefore, there are several aspects of the study that require improvement. For instance, the responses of the slope stability to irrigation should be included in the current proposed model and the horizontal displacement of station MD09 should be considered further to describe the sliding tendencies of landslides comprehensively. Furthermore, data with higher resolution, including rainfall, groundwater, and hydrological-geotechnical data, are required for more accurate predictions. All these factors will be addressed in the future and will help improve the accuracy of the proposed model.

4 Conclusions

Landslide displacement occurs under the mutual effects of numerous triggers, including the geological conditions, precipitation, and groundwater level fluctuations. In this paper, an improved KF approach considering multiple external triggers was presented for short- and mid-term landslide movement forecasting. Although the KF technique has been effective for forecasting landslide displacements since it is characterized by the best unbiased linear estimator, ease of programming, and low memory requirements, the factors triggering landside deformation are not considered, leading to poor performance. To overcome this limitation, an improved multi-factor KF technique based on the influences of external triggers was adopted to provide strong function fitting and generalization ability for improved accuracy. The model was established using more than 16 months of monitoring data from the Jingyang (China) landslide, enabling prediction of cumulative landslide displacements for periods of up to 7 months without decomposing the original displacements. Comparison revealed that the developed model performed better than the improved single-factor KF method, single-factor KF model, multi-factor KF technique, and traditional approaches such as the RBF and SVR models when applied to the study region. The *RMSE*, *MAPE*, and R^2 values of the proposed approach were found to be 4.608 mm, 0.7%, and 0.976, respectively. Given the random disturbances of external factors, the improved multi-factor KF approach can accurately simulate the relationships between the triggering factors and landslide deformation. Moreover, the predictions obtained using the proposed method were found to be stable, which is crucial for early landslide prevention. Further, the proposed technique can be constantly updated with new measurements and applied to other landslide-prone regions, providing reliable information for early landslide warning systems.

Nevertheless, the effects of variations in groundwater level caused by irrigation and seasonal freeze–thaw will play an important role in improving the performance of the proposed model. Therefore, the exact effects of these factors will be investigated in future research using the necessary monitoring equipment. Modeling the horizontal displacement to comprehensively describe the sliding trends of landslides will also be considered in the future. The model developed in this study can be applied to landslide movements triggered by rainfall; it is not appropriate for forecasting landslide deformations induced by internal triggers, earthquakes, or other types of seismic movements.

Acknowledgements The authors are grateful to surveyors who work hard around the Jingyang in a challenging environment to obtain Monitoring data. This study is also supported. by the National Natural Science Foundation of China (Grant Nos. 41731066, 41674001, 41790445), the Natural Science Basic Research Plan in Shaanxi Province of China (No. 2019JM-202), the Special Fund for Basic Scientific Research of Central Universities (No. CHD300102268204), the Fundamental Research Funds for the Central Universities (No. CHD300102269104), the Natural Science Foundation in Gansu Province of China (No. 2017GS10845). We thank Professor Li Wang (Chang'an University) for conducting the measurement. Constructive

comments from editor and two anonymous reviewers improved the manuscript.

References

Alimohammadlou Y, Najafi A, Gokceoglu C (2014). Estimation of rainfall-induced landslides using ANN and fuzzy clustering methods: a case study in Saeen Slope, Azerbaijan province, Iran. Catena, 120: 149–162

An H, Viet T T, Lee G, Kim Y, Kim M, Noh S, Noh J (2016). Development of time-variant landslide-prediction software considering three-dimensional subsurface unsaturated flow. Environ Model Softw, 85: 172–183

Bai S, Wang J, Zhang Z, Cheng C (2012). Combined landslide susceptibility mapping after Wenchuan earthquake at the Zhouqu segment in the Bailongjiang Basin, China. Catena, 99:18–25

Bui D, Tuan T, Klempe H, Pradhan B, Revhaug I (2016). Spatial prediction models for shallow landslide hazards: a comparative assessment of the efficacy of support vector machines, artificial neural networks, kernel logistic regression, and logistic model tree. Landslides, 13(2): 361–378

Carlà T, Intrieri E, Farina P, Casagli N (2017). A new method to identify impending failure in rock slopes. Int J Rock Mech Min, 93: 76–81

Cao Y, Yin K L, Alexander D E, Zhou C (2016). Using an extreme learning machine to predict the displacement of step-like landslides in relation to controlling factors. Landslides, 13(4): 725–736

Chen W, Wang J L, Xie X S, Hong H Y, Trung N V, Bui D T, Wang G, Li X R (2016). Spatial prediction of landslide susceptibility using integrated frequency ratio with entropy and support vector machines by different kernel functions. Environ Earth Sci, 75(20): 1344

Cojean R, Caï Y J (2011). Analysis and modeling of slope stability in the Three Georges Dam Reservoir (China)—the case of Huangtupo landslide. J Mt Sci, 2(8): 166–175

Colkesen I, Sahin E K, Kavzoglu T (2016). Susceptibility mapping of shallow landslides using kernel-based Gaussian process, support vector machines and logistic regression. J Afr Earth Sci, 118: 53–64

Crosta G B, Agliardi F (2003). Failure forecast for large rock slides by surface displacement measure. Can Geotech J, 40(1):176–191(16)

Cui X Z, Yu Z S, Tao B Z, Liu D J, Yu Z L (2009). Generalized Adjustment. Wuhan: Wuhan University Press

De Livera A M, Hyndman R J, Snyder R D (2011). Forecasting time series with complex seasonal patterns using exponential smoothing. J Am Stat Assoc, 106(496): 1513–1527

Duang Z (2013). Study on the trigger mechanism of loess landslide. Dissertation for the Doctoral Degree. Xi'an: Chang'an University

Fu J (2013). Application of Kalman filter method in landslide deformation forecast. Dissertation for the Doctoral Degree. Wuhan: China University of Geosciences

Fukuzono T (1985). New methods for predicting the failure time of a slope. In: Proceedings of the 4th International Conference and Field Workshop on Landslides. Tokyo: Tokyo University Press, p145–150

Gao W, Feng X (2006). Study on displacement predication of landslide based on grey system and evolutionary neural network. Computer Methods Eng Sci, 890–894

He Y (2016). Identification and monitoring of the loess landslide by using of high resolution remote sensing and InSAR. Dissertation for the Doctoral Degree. Xi'an: Chang'an University

He K Q, Wang S Q, Du W, Wang S J (2010). Dynamic features and effects of rainfall on landslides in the Three Gorges Reservoir region, China: using the Xintan landslide and the large Huangya landslide as the examples. Environ Earth Sci, 59(6): 1267–1274

Hong H Y, Pradhan B, Jebur M N, Bui D T, Xu C, Akgun A (2016). Spatial prediction of landslide hazard at the Luxi area (China) using support vector machines. Environ Earth Sci, 75(1): 40

Huang R (2004) On time predication of landslide. Scientific and Technological Management of Land and Resources, (06):15–20

Huang R (2007). Large-scale landslides and their sliding mechanisms in China since the 20th Century. Chinese Journal of Rock Mechanics and Engineering, 26(03): 433–454

Huang F M, Yin K L, Zhang G R, Gui L, Yang B B, Liu L (2016). Landslide displacement prediction using discrete wavelet transform and extreme learning machine based on chaos theory. Environ Earth Sci, 75(20): 1376

Jing Y L, Dai F C (2007). The mechanism of irrigation-induced landslides of loess. Chinese Journal of Geotechnical Engineering, 10: 1493–1499

Krkač M, Špoljarić D, Bernat S, Arbanas S M (2017). Method for prediction of landslide movements based on random forests. Landslides, 14(3): 947–960

Li C, Fan L, Zhang J, Miao S, Wang Y (2010). Application of Kalman filtering to high and steep slope deformation monitoring prediction of open-pit mines. J Univ Sci Technol Beijing, 32(01): 8–13

Li R P, Shi H B, Chi J G, Zhang Y Q(2007). Characteristics of air temperature and water-salt transfer during freezing and thawing period. Transactions of the Chinese Society of Agricultural Engineering, 23(04): 70–74

Li X, Kong J, Wang Z (2012). Landslide displacement prediction based on combining method with optimal weight. Nat Hazards, 61(2): 635–646

Li Y, Li C, Yan C, Zeng Y (2008). Application of multivariable time series based on RBF neural network in prediction of landslide Displacement. In: Proceedings of 2008 International Workshop on Chaos-Fractals Theories and Applications & the 9th International Conference for Young Computer Scientists, 2707–2712

Liu Z, Gu T, Kang X (2017). The influence of the rising of groundwater level on the stability of loess slope. Ground Water, 39(6):61–63 + 162

Liu Z, Shao J, Xu W, Chen H, Shi C (2014). Comparison on landslide nonlinear displacement analysis and prediction with computational intelligence approaches. Landslides, 11(5): 889–896

Lu F, Jiang T (2017). The deformation forecast model of landslides based on multiple factors and taylor series. Journal of Geodesy and Geodynamics, (37): 1029–1032

Miao F, Wu Y, Xie Y, Li Y (2018). Prediction of landslide displacement with step-like behavior based on multi algorithm optimization and a support vector regression model. Landslides, 15(3): 475–488

Polykretis C, Ferentinou M, Chalkias C (2015). A comparative study of landslide susceptibility mapping using landslide susceptibility index and artificial neural networks in the Krios River and Krathis River catchments (northern Peloponnesus, Greece). Bull Eng Geol Environ, 74(1): 27–45

Pradhan B, Lee S (2010). Regional landslide susceptibility analysis using back-propagation neural network model at Cameron Highland, Malaysia. Landslides, 7(1): 13–30

Pradhan B (2013). A comparative study on the predictive ability of the decision tree, support vector machine and neuro-fuzzy models in landslide susceptibility mapping using GIS. Comput Geosci, 51: 350–365

Qian H, Lei G, Yu P (2012). Multiple fading factors Kalman filter and its application in SINS initial alignment. J Chin Inert Technol, 20: 287–291

Saito M (1965). Forecasting the time of occurrence of a slope failure. In: Proceedings of 6th International Congress of Soil Mechanics and Foundation Engineering, Montreal: 537–541

Tazik E, Jahantab Z, Bakhtiari M, Rezaei A, Alavipanah S K (2014). Landslide susceptibility mapping by combining the three methods fuzzy logic, frequency ratio and analytical hierarchy process in Dozain basin. Int Arch Photogramm Remote Sens Spat Inf Sci, XL-2 (W3): 267–272

Voight B (1988). A method for prediction of volcanic eruptions. Nature, 332(6160): 125–130

Voight B (1989). A relation to describe rate-dependent material failure. Science, 243(4888): 200–203

Wang N, Yao Y (2008). Characteristics and mechanism of landslides in loess during freezing and thawing periods in seasonally frozen ground regions. Journal of Disaster Prevention and Mitigation Engineering, 28(02): 163–166

Wu Y, Teng W, Li Y (2007). Application of grey-neural network model to landslide deformation prediction. Chinese Journal of Rock Mechanics and Engineering, 26(03): 632–636

Xu C, Dai F C, Xu X, Lee Y H (2012). GIS-based support vector machine modeling of earthquake-triggered landslide susceptibility in the Jianjiang River watershed, China. Geomorphology, 145–146: 70–80

Xu S L, Niu R Q (2018). Displacement prediction of Baijiabao landslide based on empirical mode decomposition and long short-term memory neural network in Three Gorges area, China. Comput Geosci, 111: 87–96

Xu Y, Tang Y, Li X, Ye G (2011). The landslide deformation prediction with improved Euler method of gray system model GM(1,1). Hydrogeology Eng Geol, 38(1): 110–113

Yalcin A, Reis S, Aydinoglu A C, Yomralioglu T (2011). A GIS-based comparative study of frequency ratio, analytical hierarchy process, bivariate statistics and logistics regression methods for landslide susceptibility mapping in Trabzon, NE Turkey. Catena, 85(3): 274–287

Yan T (1988). Statistical prediction method of landslide. In: Landslide Anthology. Beijing: China Railway Publishing House

Yang Y X, He H, Xu G (2001). Adaptively robust filtering for kinematic geodetic positioning. J Geod, 75(2-3): 109–116

Yang Y X, Gao W (2006). An optimal adaptive Kalman filter. J Geod, 80(4): 177–183

Yang Y X, Gao W, Zhang X (2010). Robust Kalman filtering with constraints: a case study for integrated navigation. J Geod, 84(6): 373–381

Zhang J, Liu Z Q, Wang H, Zhang Z L (2012). Landslide deformation monitoring analysis and forecast using Kalman filtering considering rainfall. Science of Surveying and Mapping, 37(6): 58–61

Zhang J, Yin K L, Wang J, Huang F (2015). Displacement prediction of baishuihe landslide based on time series and PSO-SVR model. Chinese Journal of Rock Mechanics and Engineering, 34(2): 382–391

Zhou C, Yin K L, Cao Y, Intrieri E, Ahmed B, Catani F (2018). Displacement prediction of step-like landslide by applying a novel kernel extreme learning machine method. Landslides, 15(11): 2211–2225

Zou Z X, Xiong C G, Tang H M, Criss R E, Su A, Liu X (2017). Prediction of landslide runout based on influencing factor analysis. Environ Earth Sci, 76(21): 723